ACS OMEGA

http://pubs.acs.org/journal/acsodf

Article

# Study on the Construction of Dopamine/Poly(ethyleneimine)/Aminoated Carbon Nanotube Multilayer Films on Aramid Fiber Surfaces to Improve the Mechanical Properties of Aramid Fibers/Epoxy Composites

Ting Xu, Jin Tian, Lizhou An,* Yumin Jiao, Qin Yin, and Yefa Tan

Cite This: *ACS Omega* 2022, 7, 35610−35625

Read Online

ACCESS | Metrics & More | Article Recommendations

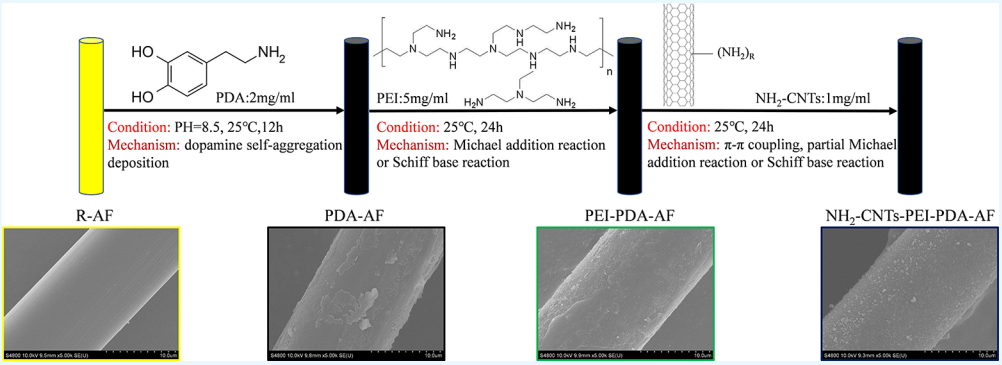


**ABSTRACT:** To improve the mechanical properties of aramid fiber (AF) reinforced epoxy resin (EP) composites without damaging the strength of the AF body, in this paper, poly(ethyleneimine) (PEI) and aminoated carbon nanotubes ($NH_2$-CNTs) were successfully deposited on the AF surface layer by layer using poly(dopamine) (PDA) as the initial layer. The modified aramid fibers PDA-AF, PEI-PDA-AF, and $NH_2$-CNTs-PEI-PDA-AF were prepared. The microstructure and chemical composition of the AF surface at different modification stages were systematically characterized. The interfacial properties, mechanical properties, and strengthening mechanism of AF surface-modified composites were studied. The results showed that with the successful deposition of PDA, PEI, and $NH_2$-CNTs layer by layer, the interfacial properties and mechanical properties of the composites gradually improved. Among them, $NH_2$-CNTs-PEI-PDA-AF showed the best strengthening effect. Compared with the unmodified aramid fiber (R-AF), the monofilament tensile strength of $NH_2$-CNTs-PEI-PDA-AF increased by 8.1%, the contact angle with EP decreased by 21.9%, and the interface energy and adhesion energy increased by 115 and 21.4%, respectively. Compared with R-AF/EP, the interlaminar shear strength (ILSS), bending strength, and tensile strength of $NH_2$-CNTs-PEI-PDA-AF/EP were increased by 75, 44.5, and 14.9%, respectively. The significant improvement of the interface properties and mechanical properties between $NH_2$-CNTs-PEI-PDA-AF and EP can be attributed to the introduction of a large number of amino active groups in the $NH_2$-CNTs-PEI-PDA coating layer on the AF surface, which strengthens the chemical-bond cooperation between the AF and EP matrix. At the same time, a large number of $NH_2$-CNTs deposited on the surface effectively increased the surface roughness of AF, improved the mechanical meshing between the AF and EP matrix, and then improved the contact angle, surface energy, and interface bonding strength between the AF and EP matrix. Moreover, a large number of $NH_2$-CNTs on the surface of AF also modified and enhanced the EP in the interface region, which could make the load more effectively transfer from the resin to the fiber, so that AF could carry the load more uniformly, significantly improving the mechanical properties of $NH_2$-CNTs-PEI-PDA-AF/EP.

## 1. INTRODUCTION

Aramid fiber is a kind of organic fiber composed of an aromatic ring and an amide bond on the main chain of a macromolecule. It has a series of excellent properties such as high specific modulus, high specific strength, low density, and high wear resistance. As the reinforcement material of advanced composite materials, it is widely used in aerospace, military protection, mechanical vehicles, and many other fields.[1−4] For

Received: May 31, 2022
Accepted: August 31, 2022
Published: September 29, 2022





https://doi.org/10.1021/acsomega.2c03390
*ACS Omega* 2022, 7, 35610−35625

example, in aviation, in order to reduce mass and improve economic efficiency, aramid composite materials are used in commercial aircraft and helicopters: the total amount of aramid composite materials on the L-1011 Samsung passenger aircraft has reached 1135 kg, which reduces the weight of the aircraft by 365 kg; the exterior surface of the S-76 commercial helicopter is made up of 50% aramid fiber composite materials. In aerospace, it is used in rocket engine casing, pressure vessels, spacecraft cockpits, etc. In the military field, it is used in the bulletproof plate of tanks, armored vehicles, aircraft, and boats, as well as in helmets and bulletproof vests. In the field of mechanical vehicles, aramid fibers, instead of a steel cord, are widely used in tires because of their lighter weight and less rolling resistance. However, the high degree of orientation and crystallinity, smooth surface, high inertness, and low reactivity of aramid fibers led to their wetness being poor and their interfacial bonding property with the polymer matrix being poor too, limiting the full play of their enhancement performance to a certain extent.[5,6] Therefore, an important technical way to improve the mechanical properties of aramid fiber-reinforced epoxy composites is using surface modification technology to modify the surface of the aramid fiber appropriately in order to improve the interface properties between the aramid fiber and the epoxy matrix.

At present, surface modification methods of aramid fibers mainly include surface oxidation technology, high-energy ray technology, vapor deposition (CVD) coating technology, and surface grafting technology.[7−13] Compared with other surface modification treatment techniques, the chemical graft modification technology has a unique advantage: it not only retained the excellent properties of the fiber itself but also gave some new properties to the fiber surface through the grafted side chain. Moreover, the method is easy to operate, easy to realize the reaction conditions, and low cost, so it is widely favored by researchers and has become a research focus in the field of fiber surface modification.

In recent years, carbon nanotubes (CNTs) have shown great potential in modifying high-performance fibers to enhance their interface properties with the matrix due to their excellent mechanical properties and good chemical and thermal stability. For example, Zhao[14] introduced amine-functionalized CNTs on the surface of carbon fibers. The introduction of CNTs effectively increased the fiber surface roughness, deflected and blocked cracks, increased the cracking area between the fiber and the resin, and consumed more energy. The interfacial strength and impact toughness of the grafted carbon fiber/epoxy resin composites were both improved obviously. Mei[15] grafted carboxylated carbon nanotubes onto the surface of carbon fiber and studied the microscopic morphology and surface energy of this multiscale reinforcement. The results show that the surface roughness of the carbon nanotube/carbon fiber multiscale reinforcement is about 260% higher than that of the carbon fiber filament. In addition, the carbon fiber surface polar component after grafting of CNTs was also increased, and the interfacial property between the fiber and the matrix improved obviously. Yang[16] achieved carboxylated carbon nanotube graft on the surface of aramid fibers based on the Friedel−Crafts reaction. The fiber surface was rougher, the wettability and surface energy were improved significantly, a higher bonding strength was generated with the rubber matrix, and the extraction force between the aramid fiber and the rubber matrix increased by about 46.3% compared with the unmodified aramid fiber. However, most of the pretreatment or the initial graft-layer selection of the above-mentioned methods involves strong acids and toxic solvents, which damage the chemical and crystal structure of the fiber surface to a certain extent, leading to the decline of fiber body strength. Therefore, it is very important to explore a green method to introduce carbon nanotubes onto the aramid fiber surface without damaging the fiber body strength.

Dopamine (DA) surface modification is a new kind of surface modification method of grafted polymers emerging in recent years. The deposition process is mild, easy to operate, and does not damage the matrix material. It can be spontaneously carried out in weakly alkaline, normal-temperature, and air-atmosphere conditions. Thanks to the catechol groups in the poly(dopamine) (PDA) structure, dopamine self-aggregation deposition has substrate universality, it has superadhesion properties, and it can be easily deposited on almost all types and sizes of inorganic and organic substrates with controllable coating thickness and durable stability.[17−19] In addition, the deposited PDA layer has functional groups such as hydroxyl and imine groups, which can form covalent bonds with thiols and amines through the Michael addition reaction or the Schiff base reaction in a mild environment.[20−22] Therefore, dopamine was chosen as the initial layer to realize the surface modification of the aramid fiber by a carbon tube.

However, it is well known that the strong intermolecular force between carbon tubes makes it easy to produce irreversible agglomeration in a solution.[23−25] It is also very important to introduce active points uniformly on the fiber surface and make CNTs grafted on the fiber surface uniformly and regularly dispersed. Poly(ethyleneimine) (PEI) is a type of partial branched polymer containing a primary amine, a secondary amine, and a tertiary amine. The amino group on the highly adsorptive and attached PEI branched chain can react with the hydroxyl group to form a hydrogen bond, react with the carboxyl group to form an ionic bond, and react with the carbonyl group to form a covalent bond. Because PEI contains polar groups (amino) and hydrophobic groups (vinyl), it can be combined with different substances. In particular, PEI molecules with many branched chains have great steric hindrance, which can hinder the adsorption and agglomeration between carbon nanotubes.[26] Therefore, on the basis of dopamine as the initial layer, poly(ethyleneimine) was selected as the transition layer to further realize the surface modification of aramid fibers by a carbon tube.

Although the modification effect of dopamine on aramid fibers has been analyzed in previous studies, the surface modification of aramid fibers by carbon nanotubes using dopamine and poly(vinyl imide) as initial and transition layers has not been reported.

Therefore, in this paper, self-polymerization deposition of PDA was used as the initial layer of aramid fiber (AF) surface modification, and the PEI transition layer was deposited by means of PDA's superadhesion, the Michael addition reaction, or the Schiff base reaction. On this basis, aminoated carbon nanotubes ($NH_2$-CNTs) were further grafted by $\pi-\pi$ coupling, the partial Michael addition reaction, or the Schiff base reaction. The modified aramid fibers PDA-AF, PEI-PDA-AF, and $NH_2$-CNTs-PEI-PDA-AF were prepared separately. The purpose of this paper is to introduce active functional groups into the surface of AF, increase its surface activity and surface roughness, improve the wetted properties of the fiber and the interface properties between the fiber and the resin, and improve the mechanical properties of fiber composites.


https://doi.org/10.1021/acsomega.2c03390
ACS Omega 2022, 7, 35610−35625

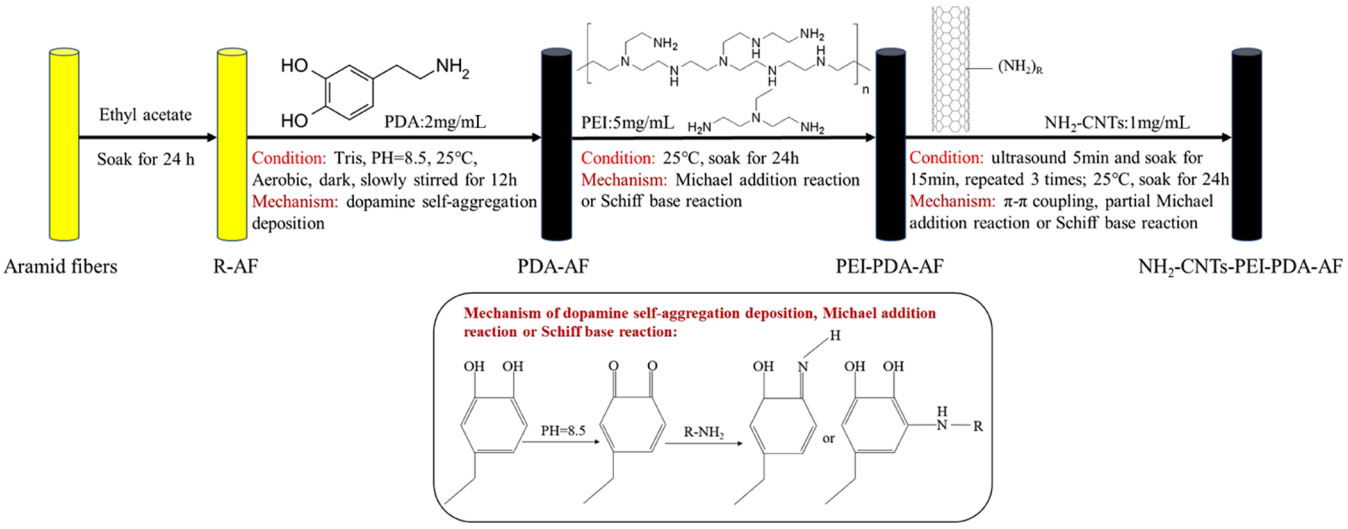


**Figure 1.** Preparation process and reaction mechanism of AF surface modification.

The surface morphology of AF was observed by scanning electron microscopy (SEM). The surface groups and chemical composition of AF were characterized by Fourier transform infrared spectroscopy (FTIR), thermogravimetric analysis (TGA), and X-ray photoelectron spectroscopy (XPS). The wettability of AF was measured by static contact angle analysis, and the interfacial energy and adhesion work were calculated. The tensile strength of AF monofilaments and the interlaminar shear strength (ILSS) between AF and the epoxy resin (EP) matrix were tested, the bending strength and tensile strength of AF/EP composites at different modification stages were tested, and the strengthening mechanism of AF/EP composites was studied, which provided technical support for further research and development and engineering applications of aramid fiber-reinforced epoxy resin composites.

## 2. EXPERIMENTAL SECTION

**2.1. Experimental Materials.** Aramid fiber (AF), model: Kevlar-29; average diameter 14 $\mu$m. Aramid fiber cloth, model: XL-AF480B-100; square gram weight 480 g cm$^{-2}$; width 100 cm; DuPont 1500 D, K29 fiber, Yixing Xinli Weaving Co., Ltd.; aminoated carbon nanotubes ($NH_2$-CNTs), outer diameter 8−15 nm, length of about 50 $\mu$m, amino content of about 0.45 wt %, Nanjing Xianfeng Nanomaterials Technology Co., Ltd.; dopamine hydrochloride (DA), Tris (hydroxymethyl) aminomethane (Tris), ethyl acetate, poly-(ethyleneimine) (PEI), deionized water, Shanghai Aladdin Biochemical Technology Co., Ltd.; IN2 guide epoxy resin, AT300SLOW curing agent, Beijing Composite Yigou Technology Co., Ltd. (IN2/AT300SLOW = 100:30).

**2.2. Surface Modification Process of Aramid Fibers.** To improve the surface roughness and wettability of AF, the surface of AF was chemically grafted to prepare modified aramid fibers PDA-AF, PEI-PDA-AF, and $NH_2$-CNTs-PEI-PDA-AF, separately. The specific process is as follows.

*2.2.1. AF Surface-Deposited PDA Initial Layer.* First, AF (length of each fiber bundle was 20 cm) was soaked in ethyl acetate for 24 h for surface pretreatment to remove impurities from the fiber surface. Then, it was cleaned with deionized water three times and dried in an oven at 60 °C for 12 h. After drying, AF was denoted as R-AF.

A total of 200 mL of deionized water was added with 0.2422 g of Tris and 0.4 g of DA to prepare a 2 mg mL$^{-1}$ dopamine solution (pH = 8.5). R-AF was placed in a dopamine solution, and then, under aerobic conditions, avoiding light, and at room temperature, it was mixed for 12 h using a magnetic blender (stirring speed 50 rpm). Then, the fiber bundle was removed by washing with deionized water three times until the filtrate became colorless and transparent, so as to remove unreacted dopamine from the fiber surface, and finally, it was placed in a 60 °C oven for drying for 12 h. After drying, AF with PDA deposited on the surface was obtained, which was denoted as PDA-AF.

*2.2.2. PDA-AF Surface-Deposited PEI Transition Layer.* PDA-AF was immersed in a PEI water solution with a concentration of 5 mg mL$^{-1}$ and soaked at room temperature for 24 h. PEI was further deposited on the surface of AF by the Michael addition reaction or the Schiff base reaction. After the reaction, the fibers were washed with deionized water three times and then dried in an oven at 60 °C for 12 h. After drying, PDA-AF with the PEI transition layer deposited on the surface could be obtained, denoted as PEI-PDA-AF.

*2.2.3. PEI-PDA-AF Surface-Grafted $NH_2$-CNTs.* The $NH_2$-CNT aqueous solution with a concentration of 1 mg mL$^{-1}$ was prepared, which was stirred and treated with ultrasound at room temperature for 5 min. The prepared PEI-PDA-AF was immersed in a $NH_2$-CNT aqueous solution for 15 min. Then, the fibers were removed, the $NH_2$-CNT aqueous solution was treated with ultrasound again for 5 min, and the fibers were immersed in the $NH_2$-CNT aqueous solution again for 15 min. This was repeated three times, and then, the fibers were immersed in the $NH_2$-CNT aqueous solution for 24 h. The fibers were removed and washed three times with deionized water to remove excess $NH_2$-CNTs. Finally, the fibers were dried in an oven at 60 °C for 12 h. After drying, fibers grafted with $NH_2$-CNTs were obtained, denoted as $NH_2$-CNTs-PEI-PDA-AF.

The preparation process and reaction mechanism of AF surface modification are shown in Figure 1.

**2.3. Testing and Characterization.** A scanning electron microscope (SEM) (Hitachi S-4800, Hitachi, Japan) was used to observe the AF surface morphology. Before observation, the sample was treated with gold-spraying and the acceleration


https://doi.org/10.1021/acsomega.2c03390
ACS Omega 2022, 7, 35610−35625

voltage was 10 KV. A Fourier transform infrared spectrometer (FTIR) (PerkinElmer Spectrum Two, Waltham, Massachusetts) was used to analyze the AF surface functional groups. The scanning resolution and scanning frequency were 4 $cm^{-1}$ and 32 times, respectively, and the scanning range was 400−4000 $cm^{-1}$. A thermal gravimetric analyzer (TGA) (209 F3 Tarsus, Selb, Germany) was used to analyze the AF thermal stability in a nitrogen atmosphere at the heating rate of 10 °C $min^{-1}$ and the maximum heating temperature of 800 °C. The surface chemical composition, relative content, and elemental binding morphology of AF were analyzed by X-ray photoelectron spectroscopy (XPS) (ESCALAB 250XI, Waltham, Massachusetts). The C 1s peak (284.8 eV) was selected to correct the energy displacement of each element's narrow sweep spectrum, and peak-differentiating and imitating were performed by Advantage software. A contact angle measuring instrument (DSA100, Kruss, Germany) was used to measure the static contact angle of AF and analyze the wettability and surface energy of AF. The microdroplet method was used for testing. The test liquid adhered to the surface of the monofilament in the form of a spray and formed microdroplets with a volume of about 5 μL. After the droplet was stabilized, the contact angle was fitted by Young−Laplace software.

Based on the GB/T 31290-2014 standard, the tensile strength of the AF monofilament in different modification stages was tested, and the influence of the modification process on the tensile strength of the AF monofilament was studied. Figure 2 is a schematic diagram of the AF monofilament tensile

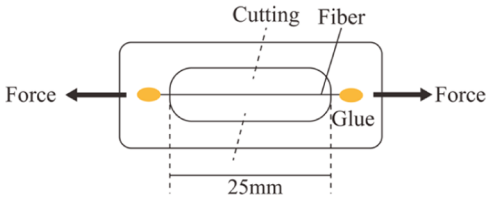


**Figure 2.** Diagram of the AF monofilament tensile strength test.

strength test. First, thin paper with a thickness of 0.1 mm was used to make a thin sheet with a slot of 25 mm ± 0.5 mm in length. The single fiber was then stretched and fixed on the centerline of the test paper frame, and both ends were bonded with 101 adhesive. The paper frame was fixed in the fixture of the testing machine, the paper frame (along the cutting line in the figure) was cut, the loading rate was 1 mm $min^{-1}$, and the maximum load was recorded.

The AF monofilament tensile strength can be calculated by formula 1

$$\sigma_f = \frac{4F_{max}}{\pi d^2} \quad (1)$$

where $\sigma_f$ represents the AF monofilament tensile strength, $F_{max}$ represents the maximum load when AF breaks, and $d$ represents the AF monofilament diameter.

Aramid fiber-reinforced epoxy resin matrix composites were prepared by the vacuum conductivity method. The interlaminar shear strength (ILSS) of composite plates was tested on an electronic universal testing machine CMT 5105 according to ASTM D2344 using the three-point short beam bending method. The test was carried out at room temperature, the sample size was 15 mm × 5 mm × 3 mm, the span thickness ratio was 4:1, and the loading speed of the indenter was 1 mm $min^{-1}$. Five valid data were selected from each group of samples, and their average value was taken. The formula for calculating the ILSS of composite materials is shown in eq 2

$$\tau = \frac{3P_b}{4bh} \quad (2)$$

In the formula, $\tau$ is the ILSS value of the composite (unit MPa), $P_b$ is the maximum load borne by the sample (unit N), $b$ is the width of the sample (unit mm), and $h$ is the thickness of the sample (unit mm).

According to the ASTM D7264 standard, the three-point bending method was used to test the bending properties of the composite sheet metal on the electronic universal testing machine CMT 5105. The test was carried out at room temperature, the sample size was 60 mm × 15 mm × 3 mm, the span thickness ratio was 16:1, and the loading speed of the indenter was 5 mm $min^{-1}$. Five valid data were selected from each group of samples, and their average value was taken. The formula for calculating the bending strength of composite materials is shown in formula 3

$$\sigma_B = \frac{3P_{max}L}{2\omega h^2} \quad (3)$$

In the formula, $\sigma_B$ is the bending strength of the composite material (unit MPa), $P_{max}$ is the maximum load borne by the sample (unit N), $L$ is the span (unit mm), $\omega$ is the width of the sample (unit mm), and $h$ is the thickness of the sample (unit mm).

The tensile strength of the composite sheet is tested on an electronic universal testing machine UTM 5504 according to ASTM D3039. The test was carried out at room temperature with the sample size of 250 mm × 25 mm × 3 mm. Aluminum alloy reinforcement plates were used in the test, and the size of reinforcement plates was 50 mm × 25 mm × 2 mm. The beam displacement rate was 5 mm $min^{-1}$. Five valid data were selected from each group, and their average value was taken. The formula for calculating the tensile strength of composite materials is shown in eq 4

$$\sigma_t = \frac{P^{max}}{A} \quad (4)$$

In the formula, $\sigma_t$ is the tensile strength of the composite material (unit MPa), $P^{max}$ is the maximum load of the sample before failure (unit N), and $A$ is the cross-sectional area of the sample (unit $mm^2$).

The microscopic morphology of the tensile section of the composite material was observed by a KYKY-EM6900 scanning electron microscope (SEM). Before observation, the sample was treated with gold-spraying and the acceleration voltage was 20 KV.

## 3. RESULTS AND DISCUSSION

**3.1. Surface Morphology of the Aramid Fiber.** Figure 3 shows the SEM morphologies of R-AF, PDA-AF, PEI-PDA-AF, and $NH_2$-CNTs-PEI-PDA-AF. It can be seen that the surface of R-AF is smooth and neat (Figure 3a). From the high-magnification picture, it can be observed that there are some slight grooves distributed parallel to the fiber axis (Figure 3a'), which are the impressions generated during the fiber drawing process. After modification by dopamine, the surface topography of PDA-AF changed significantly (Figure 3b), its


https://doi.org/10.1021/acsomega.2c03390
ACS Omega 2022, 7, 35610−35625

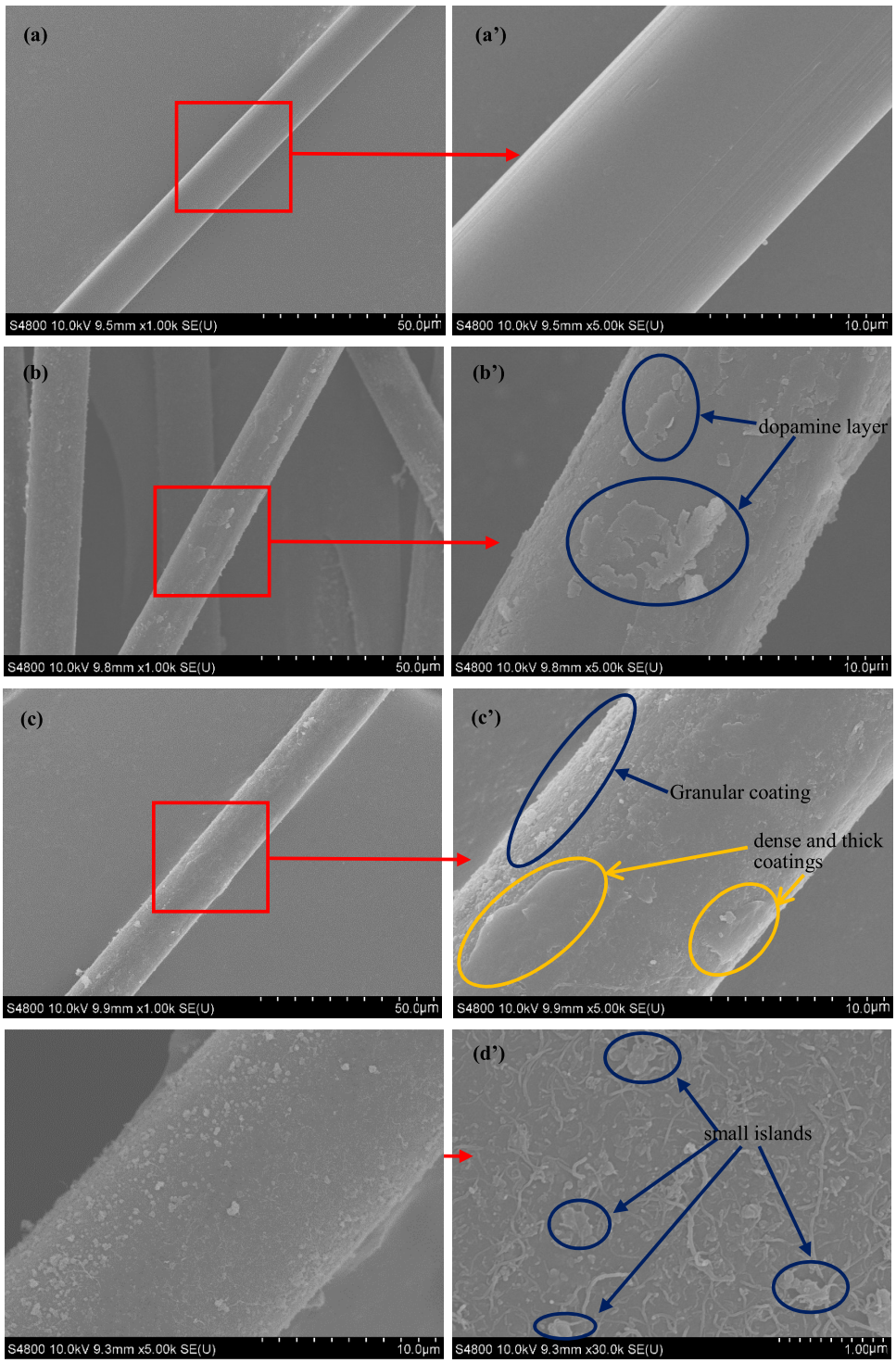


**Figure 3.** Microscopic surface morphology of AFs: (a) R-AF, (b) PDA-AF, (c) PEI-PDA-AF, and (d) $NH_2$-CNTs-PEI-PDA-AF. (a'), (b'), (c'), and (d') are the local magnified images of red-framed areas in (a), (b), (c), and (d), respectively.

surface roughness increased significantly, the grooves disappeared, and layered sediments were observed clearly (blue circled area marked in Figure 3b'), which is because the oxidative self-polymerization of dopamine leads to the formation of poly(dopamine)-layer adhesion on the fiber surface. In the process of oxidative self-polymerization of dopamine, the poly(dopamine) oligomer is formed first, and then, the oligomer forms the poly(dopamine) coating through a covalent bond, a noncovalent bond, or $\pi-\pi$ stacking.[27,28]

Compared with PDA-AF, the surface morphology of PEI-PDA-AF changed significantly, and the surface roughness increased further. Besides, a large number of granular coatings (blue circle in Figure 3c') and dense and thick coatings (yellow circle in Figure 3c') also appeared on the fiber surface. The cross-linking between the coatings resulted in a significant increase in the fiber surface coverage area, which was due to the Michael addition or Schiff base reaction between


https://doi.org/10.1021/acsomega.2c03390
ACS Omega 2022, 7, 35610−35625

poly(dopamine) and poly(ethyleneimine), which further deposited the PEI layer on the poly(dopamine) layer.

On this basis, $NH_2$-CNTs were further deposited, and the surface of the prepared $NH_2$-CNTs-PEI-PDA-AF was distributed with a large number of microconvex bodies formed by small islands of grains and blocks (the area marked by the red box in Figure 3d), which made the surface of the obtained $NH_2$-CNTs-PEI-PDA-AF more coarse, as shown in Figure 3d. From the high-magnification photo (Figure 3d'), it can be clearly observed that a large number of $NH_2$-CNTs were adsorbed on the fiber surface from various angles, with a large number, uniform distribution, and different lengths. No obvious agglomeration phenomenon of $NH_2$-CNTs was observed. Meanwhile, the large number of small islands on the fiber surface (marked by blue circles in Figure 3d') mainly comprises PDA-PEI particle coatings formed by early deposition. The dense PDA-PEI particle coating acts as a "bridge". First, $NH_2$-CNT is adsorbed on the fiber surface through $\pi-\pi$ coupling. Then, with the extension of the reaction time, a stable covalent bond can be formed between $NH_2$-CNTs and PDA-PEI particle coating through the Michael addition reaction or the Schiff base reaction, thus greatly increasing the content of $NH_2$-CNTs on the fiber surface, and firmly fixed them to the surface of the fiber. Therefore, a large number of granular and massive islands formed by PDA-PEI and a large number of uniformly distributed $NH_2$-CNTs were formed on the surface of AF after modification. On the one hand, the surface roughness of the fiber was significantly increased, which was conducive to the mechanical meshing between the AF and EP matrix to achieve the interlocking effect. On the other hand, the amino active group in $NH_2$-CNTs-PEI-PDA can chemically bond with EP, which were both conducive to the improvement of the interface bond strength and the overall mechanical properties of the composites.

**3.2. Surface Chemical Composition and Structure of the Aramid Fiber.** To analyze the changes of chemical groups on the surface of AF in different modification stages, the chemical structures of $NH_2$-CNTs and AF in different modification stages were characterized by FTIR. Figure 4 shows the FTIR spectrum of $NH_2$-CNTs. It can be seen that for $NH_2$-CNTs, there is a sharp peak at 3435 $cm^{-1}$, which is mainly caused by the stretching vibration of N−H in the primary amine group. The methylene vibration peak can be observed at 2928 $cm^{-1}$, and the peak values at 1627 and 1457 $cm^{-1}$ are generated by the N−H bending vibration and the C═C stretching vibration, respectively. In addition, the absorption peak at 1143 $cm^{-1}$ is the stretching vibration peak of C−N. Therefore, it can be confirmed that there is a certain amount of primary amine group on the $NH_2$-CNT surface.

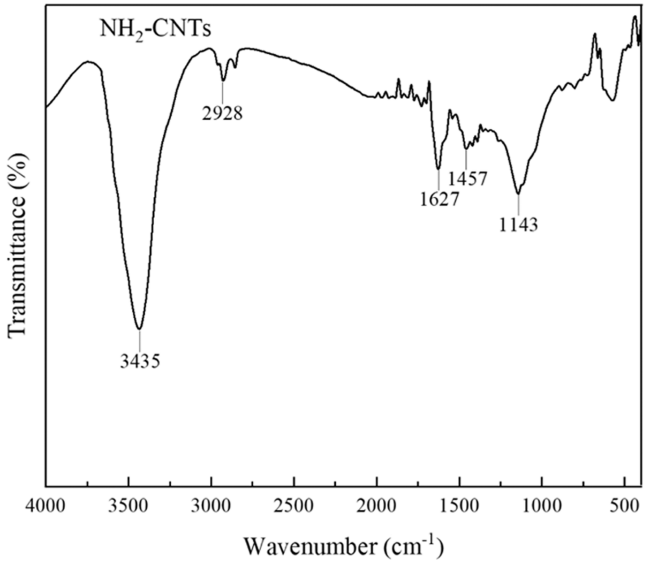


**Figure 4.** Infrared spectra of $NH_2$-CNTs.

Figure 5 shows the FTIR spectrum of AF in different modification stages. According to the FTIR spectrum of R-AF,

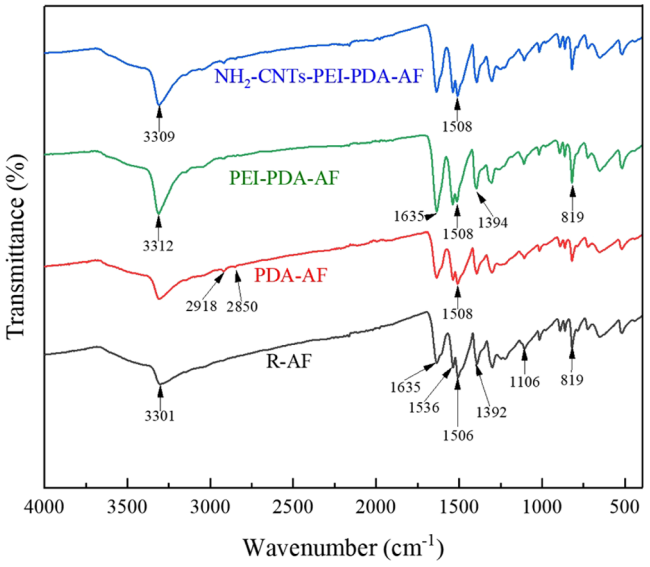


**Figure 5.** Infrared spectrogram of AF.

N−H in the amide group had peaks at 3301 and 1536 $cm^{-1}$ due to its stretching vibration and bending vibration, respectively. The peaks at 1635 and 819 $cm^{-1}$ are caused by C═O stretching vibration in the amide group and C−H bending vibration, respectively.[29,30] At the same time, the stretching vibration of C═C produces a peak at 1506 $cm^{-1}$. In addition, the two peaks at 1392 and 1106 $cm^{-1}$ are attributed to the stretching vibration of C−N. Compared with R-AF, in the FTIR spectrum of PDA-AF, the methylene stretching vibration generated new double peaks at 2918 and 2850 $cm^{-1}$, which preliminarily indicated that the PDA coating layer was successfully deposited on the AF surface.[31] At the same time, due to PDA coating, the peak at 1508 $cm^{-1}$ due to the C═C stretching vibration is slightly reduced. For PEI-PDA-AF, compared with PDA-AF, the N−H stretching vibration peak at 3312 $cm^{-1}$ could be clearly observed to increase significantly, the C═O stretching vibration peak at 1635 $cm^{-1}$ and the C−H bending vibration peak at 819 $cm^{-1}$ both increase, and the C−N stretching vibration peak at 1394 $cm^{-1}$ was slightly enhanced; these changes explain the success of the Michael addition reaction on the AF surface. Meanwhile, due to further PEI coating, the C═C stretching vibration peak at 1508 $cm^{-1}$ is further reduced. Then, the FTIR spectra of $NH_2$-CNTs-PEI-PDA-AF showed that the absorption peak at 3309 $cm^{-1}$ reduces, which could be due to the fact that $NH_2$-CNTs have fewer amino groups than PEI, and hence, XPS will be used for further analysis and research in the next step. At the


https://doi.org/10.1021/acsomega.2c03390
ACS Omega 2022, 7, 35610−35625

same time, because of the fiber surface carbon tube cladding, the C═C stretching vibration peak at 1508 $cm^{-1}$ is further increased compared to PEI-PDA-AF. According to FTIR analysis, layer-by-layer deposition of PDA, PEI, and $NH_2$-CNTs was realized on the AF surface.

The thermal decomposition process of AF in different modification stages was analyzed by the TGA test curve. Figure 6 shows the TGA test curves of $NH_2$-CNTs and AF in

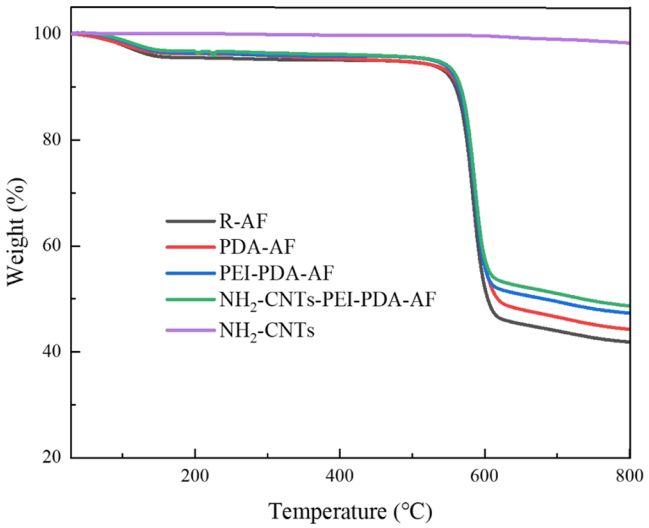


**Figure 6.** TGA curves of $NH_2$-CNTs and AF.

different modification stages. As can be seen from the figure, within the temperature range of 30−800 °C, $NH_2$-CNTs have only 1.765 wt % thermogravimetric loss, which is mainly due to the decomposition of crystal water and some unstable molecules. The tiny thermogravimetric loss indicates that $NH_2$-CNTs have excellent heat resistance. At the same time, according to the TGA curve of R-AF, the thermogravimetric loss of R-AF in the temperature range of 30−800 °C was 58.225% in total, and it decomposed sharply at 560 °C. In the temperature range of 520−620 °C, the thermogravimetric loss of R-AF was 53.709 wt %, which is mainly caused by the decomposition of partial dehydroxylation and alkoxide on AF.[32] Compared with R-AF, the thermogravimetric loss of PDA-AF and PEI-PDA-AF gradually decreased to about 55.741 and 52.8%, respectively, in the range of 30−800 °C, mainly due to the lower thermogravimetric loss of PDA (about 50 wt %) deposited on the AF surface.[10] Moreover, the relative mass of the initial PDA graft layer can be calculated to be 30%. After the fiber was further modified by the aminoated carbon tube, the thermal weight loss of $NH_2$-CNTs-PEI-PDA-AF continued to decrease to 51.445% in the range of 30−800 °C, indicating that $NH_2$-CNTs realized deposition on the AF surface (the grafting amount of $NH_2$-CNTs is 3%) and improved the heat resistance of AF.

To quantitatively analyze the composition of chemical elements and functional groups on the surface of AF, XPS tests were carried out on AF at different modification stages. Figure 7 shows the full spectrum of the XPS of AF in different modification stages. The composition of surface elements obtained from the full spectrum of XPS is listed in Table 1. Due to the high nitrogen content of dopamine (theoretical N content 9.1%), the N element content of the AF surface increased from 1.61% of R-AF to 4.41% of PDA-AF after PDA modification. The introduction of nitrogen-rich PEI molecules (theoretical N content 33.3%) further increased the N content, and the N content of PEI-PDA-AF reached 13.3%. However, the theoretical N content of the PEI-PDA copolymer is 26.9%,[33] indicating that partial copolymerization occurs in the solution and the resulting PEI-PDA copolymer does not adhere to the fiber surface.[34] After further grafting $NH_2$-CNTs, the C content on the fiber surface increased from 71.76 to 74.76%. Combined with previous SEM analysis results, it can be seen that a large number of $NH_2$-CNTs were uniformly attached to the surface of AF, and $NH_2$-CNTs were rich in C element, thus increasing the content of C element on the surface of AF. However, the N content of $NH_2$-CNTs was lower than that of nitrogen-rich PEI molecules, so the graft of $NH_2$-CNTs reduced the N content on the AF surface from 13.03 to 10.09%.

To further clarify and analyze the change in the AF surface functional group content, peak C was fitted by peak-differentiating and imitating. Figure 8 shows the C 1s split peak spectrum of AF at different modification stages, and the functional group components of the AF surface at different modification stages obtained by fitting are shown in Table 2. For R-AF, its C 1s spectrum can be fitted into four peaks, namely, C═C/C−C peak (284.7 eV), C−N peak (285.5 eV), C═O peak (287.5 eV), and O═C−O peak (288.8 eV).[35] Compared with R-AF, a new C−O peak (286.3 eV) appeared in the C 1s spectra of PDA-AF, which was due to the presence of phenolic hydroxyl groups in PDA deposited on the surface of AF. At the same time, the content of C−N increased from 11.72 to 13.48%, indicating that dopamine polymerized the AF surface. After grafting PEI by the Michael addition reaction, the C−N ratio of PEI-PDA-AF was significantly increased to 25.28% because PEI contained a large number of amino functional groups, which also confirmed the successful adhesion of PEI on the AF surface. In particular, after further grafting of $NH_2$-CNTs, the C−C/C═C content on the AF surface increased from 56.18 to 66.67% because a large number of $NH_2$-CNTs were attached on the surface of AF. These carbon tubes had a higher carbon content, so there were abundant C−C/C═C. However, the amino content of the $NH_2$-CNT itself is lower than that of PEI, so the C−N content of the AF surface decreases from 25.28 to 8% after grafting $NH_2$-CNTs. This also proved that $NH_2$-CNTs were successfully grafted onto the AF surface.

**3.3. Wettability of the Aramid Fiber and the Epoxy Resin.** The surface morphology and chemical composition of the aramid fiber affect the surface energy and its components.[36] The mechanical properties of aramid fiber-reinforced resin matrix composites are closely related to the wettability of the fiber and the epoxy. In general, good wettability means that excellent interface properties can be obtained, which helps improve the mechanical properties of composites. Contact angle is an important index to characterize the wettability of the fiber and the epoxy. By studying the changes in the contact angle between AF and EP in different modification stages, the influence rule of modification treatment on the surface wettability of AF can be explored, and the advantages and disadvantages of its wettability can be intuitively indicated.

The contact angle between AF and EP in different modification stages is shown in Figure 9. It can be seen that the contact angle between R-AF and EP is about 75.4°. After PDA and PEI modification, the contact angles of PDA-AF and PEI-PDA-AF with the EP substrate are reduced to 69.0 and


https://doi.org/10.1021/acsomega.2c03390
ACS Omega 2022, 7, 35610−35625

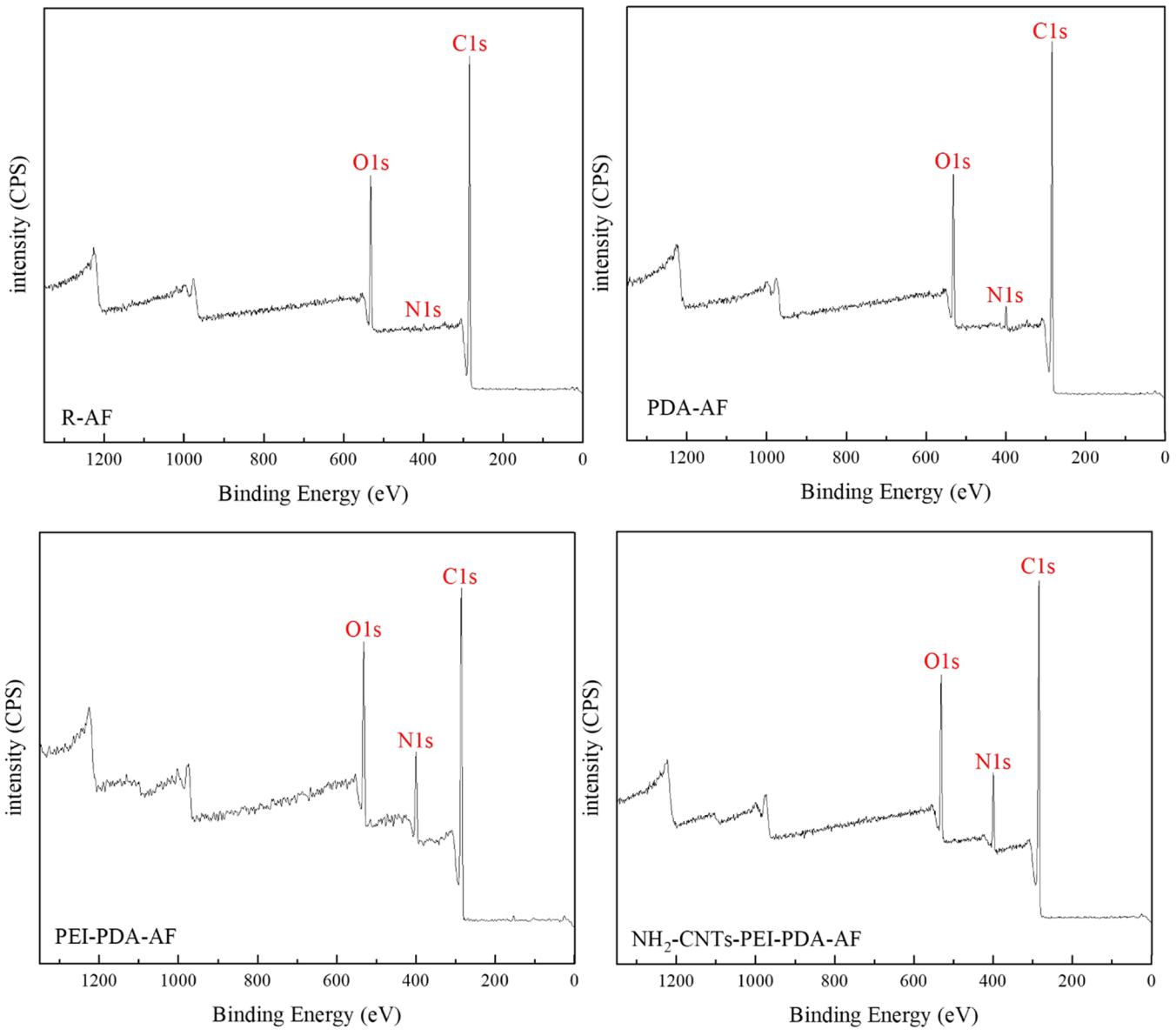


**Figure 7.** XPS full spectrum of AF.

**Table 1. Content of AF Surface Elements (%)**

| element | R-AF | PDA-AF | PEI-PDA-AF | $NH_2$-CNTs-PEI-PDA-AF |
|---|---|---|---|---|
| C | 82.13 | 79.94 | 71.76 | 74.76 |
| O | 16.27 | 15.65 | 15.21 | 15.15 |
| N | 1.61 | 4.41 | 13.03 | 10.09 |

63.6°, respectively, which are reduced by 8.5 and 15.6%, respectively, compared with R-AF. This indicated that the surface wettability of AF was improved effectively after PDA and PEI modification. On the one hand, the number of oxygen and nitrogen active functional groups on the AF surface increased due to the successful deposition of PDA and PEI, which increased the polar component of the fiber surface energy, which was conducive to the infiltration of polar liquid on the AF surface. On the other hand, the fiber surface roughness is increased by the surface-deposited coating layer, and the nonpolar component of the fiber surface energy is also increased, thus improving the wettability between the fiber and the epoxy resin.

In particular, the contact angle between $NH_2$-CNTs-PEI-PDA-AF and EP has a minimum value of 58.91°, 21.9% lower than that of R-AF. This is because a large number of carbon nanotubes are deposited on the surface of $NH_2$-CNTs-PEI-PDA-AF and their distribution is uniform. These carbon nanotubes not only further increase the surface roughness of the fiber but also have a more orderly graphite structure and higher crystallinity than the fiber surface, thus greatly improving the nonpolar component of the fiber surface energy. Therefore, the wettability between $NH_2$-CNTs-PEI-PD-AF and the epoxy matrix is better than the other.

To analyze the interfacial properties between AF and EP in different modification stages and to quantitatively analyze the AF surface energy, this paper calculated the interface energy and adhesion work of AF in different modification stages according to the Young−Dupre equation.[37] The relationship between surface energy, contact angle ($\theta$), and adhesion work is as follows

$$\gamma_{EA} = \gamma_A - \gamma_E \cos\theta \quad (5)$$



https://doi.org/10.1021/acsomega.2c03390
ACS Omega 2022, 7, 35610−35625

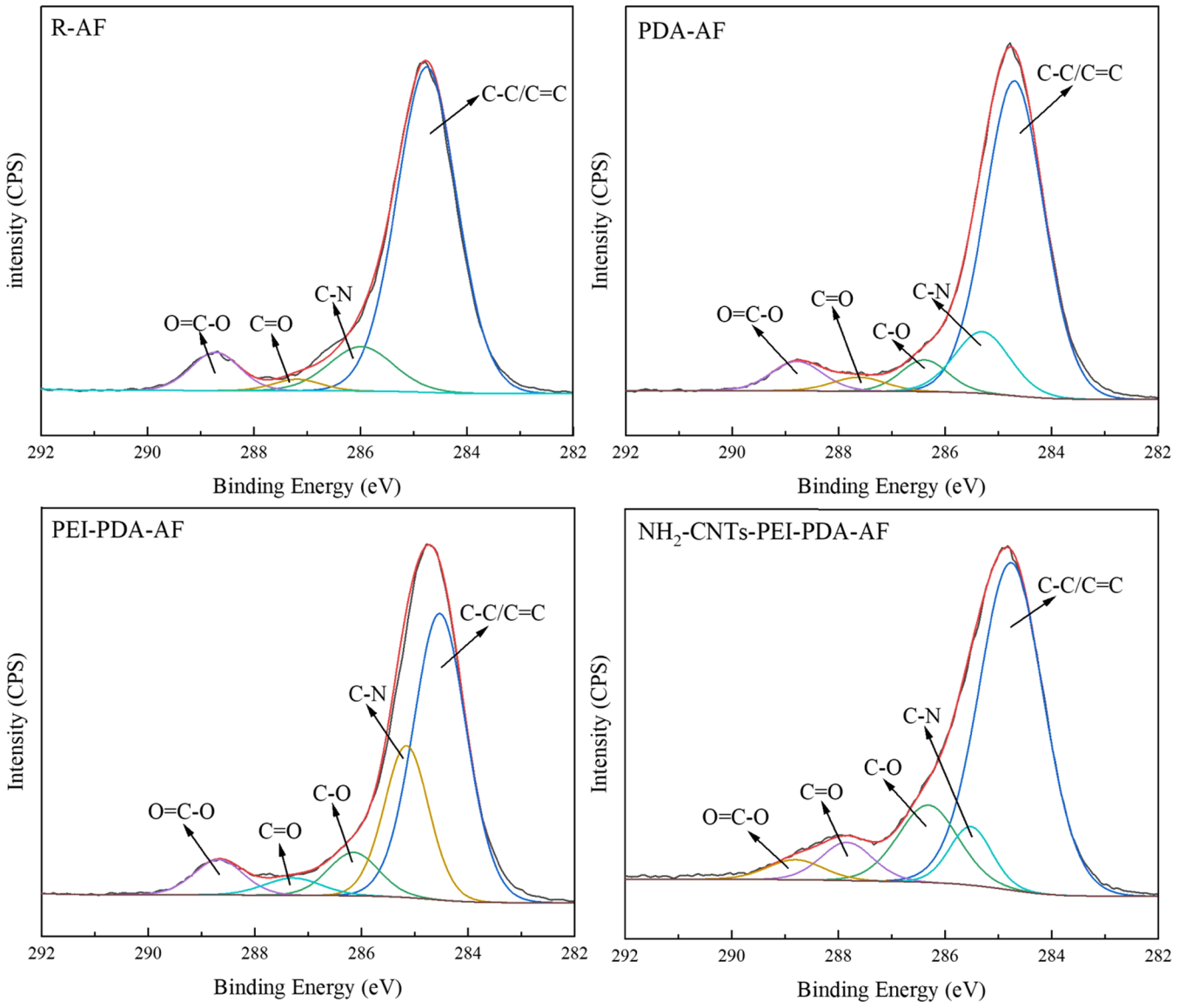


**Figure 8.** C 1s split peak spectrum of AF.

**Table 2. Composition and Content of AF Surface Functional Groups (%)**

| | content of functional groups (%) | | | | |
|---|---|---|---|---|---|
| | C−C/C=C | C−N | C−O | C=O | O=C−O |
| R-AF | 78.13 | 11.72 | | 2.34 | 7.81 |
| PDA-AF | 70.92 | 13.48 | 6.38 | 2.84 | 6.38 |
| PEI-PDA-AF | 56.18 | 25.28 | 7.87 | 3.93 | 6.74 |
| $NH_2$-CNTs-PEI-PDA-AF | 66.67 | 8.00 | 14.00 | 6.00 | 5.33 |

$$W_{EA} = \gamma_E + \gamma_A - \gamma_{EA} \quad (6)$$

In formulas 5 and 6, $\gamma_A$ is the surface energy of the aramid fiber, $\gamma_E$ is the surface energy of the epoxy resin, $\gamma_{EA}$ is the interfacial energy between the aramid fiber and the epoxy resin, and $W_{EA}$ is the adhesion work between the aramid fiber and the epoxy resin.

According to the surface energy component method of Owens and Wendt,[38] the AF surface energy and its polar and nonpolar components can be calculated from the contact angle

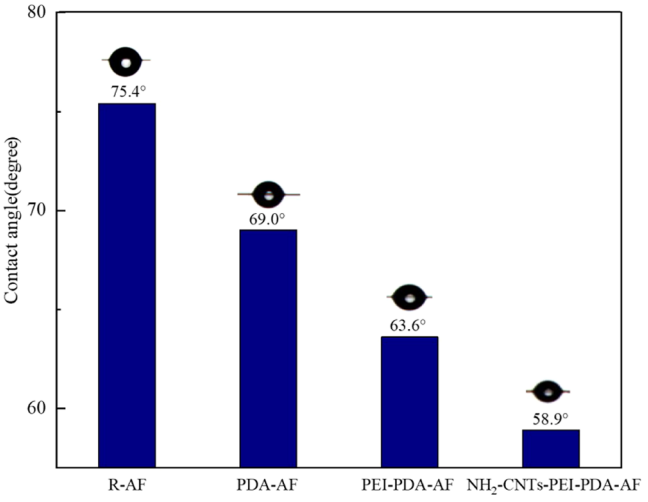


**Figure 9.** Contact angle of the EP droplet on AF.



https://doi.org/10.1021/acsomega.2c03390
ACS Omega 2022, 7, 35610−35625

($\theta$) of the aramid fiber samples in two different test fluids by the following formula.

$$\gamma_L(1 + \cos\theta) = 2\sqrt{\gamma_A^P\gamma_L^P} + 2\sqrt{\gamma_A^d\gamma_L^d} \quad (7)$$

$$\gamma_A = \gamma_A^P + \gamma_A^d \quad (8)$$

$$\gamma_L = \gamma_L^P + \gamma_L^d \quad (9)$$

In formulas 7−9, $\gamma_A$ is the surface energy of the aramid fiber, $\gamma_L$ is the surface energy of the test liquid, $\gamma_A^P$ is the polar component of the surface energy of the aramid fiber, $\gamma_A^d$ is the nonpolar component of surface energy of the aramid fiber, $\gamma_L^P$ is the polar component of surface energy of the test liquid, and $\gamma_L^d$ is the nonpolar component of surface energy of the test liquid.

According to formula 7, highly polar deionized water and nonpolar diiodomethane are selected as test liquids. The surface energy and its components of the two test liquids are shown in Table 3.

**Table 3. Surface Energy of the Test Liquid**

| | | surface energy (mJ m$^{-2}$) | | |
|---|---|---|---|---|
| test liquid type | temperature (°C) | $\gamma_L^d$ | $\gamma_L^P$ | $\gamma_L$ |
| deionized water | 20 | 21.8 | 51 | 72.8 |
| diiodomethane | 20 | 50.8 | 0 | 50.8 |

The contact angle and calculation results of the surface energy between AF and deionized water and diiodomethane in different modification stages are shown in Table 4. It can be seen that the contact angles of R-AF in deionized water and diiodomethane are 80.8 and 61.5°, respectively, and the total surface energy is low (33.9 mJ m$^{-2}$). The polar and nonpolar components of surface energy are 6.1 and 27.8 mJ m$^{-2}$, respectively. For the PDA-AF, the contact angle in the polar test liquid deionized water decreased from 80.8° of R-AF to 54.3°, and the contact angle in the nonpolar test liquid diiodomethane also decreased significantly, and the calculated surface energy increased from 33.9 mJ m$^{-2}$ of R-AF to 53.9 mJ m$^{-2}$. For PEI-PDA-AF, the contact angle in deionized water and diiodomethane both decreased further, and the contact angle in the polarity test solution decreased relatively greatly; in addition, the surface energy and its components all increased. In particular, $NH_2$-CNTs-PEI-PDA-AF has the lowest contact angle with deionized water and diiodomethane (29.6 and 24.6°, respectively), and the surface energy calculation results show that $NH_2$-CNTs-PEI-PDA-AF has the highest surface energy (72.2 mJ m$^{-2}$), which is a significant increase of 113% compared with R-AF. The high surface energy can make the polymer matrix and the fiber surface contact fully at the molecular level; effectively increase the van der Waals force, chemical bonding, and mechanical locking in the interface region; reduce the bubbles, holes, and cracks in the composite; and improve the interfacial properties between the fiber and the resin matrix. Therefore, $NH_2$-CNTs-PEI-PDA-AF showed the best wettability with the EP matrix.

**Table 4. Contact Angle and Surface Energy of Different Types of Droplets on AF**

| | contact angle (degree) | | surface energy (mJ m$^{-2}$) | | |
|---|---|---|---|---|---|
| aramid fiber | deionized water | diiodomethane | $\gamma_A^d$ | $\gamma_A^P$ | $\gamma_A$ |
| AF | 80.8 | 61.5 | 27.8 | 6.1 | 33.9 |
| PDA-AF | 54.3 | 43.8 | 37.6 | 16.4 | 53.9 |
| PEI-PDA-AF | 39.5 | 32.2 | 43.5 | 22.2 | 65.7 |
| $NH_2$-CNTs-PEI-PDA-AF | 29.6 | 24.6 | 46.3 | 25.8 | 72.2 |

Formulas 5 and 6 were used to further calculate the interfacial energy and adhesion work between R-AF, PDA-AF, PEI-PDA-AF, and $NH_2$-CNTs-PEI-PDA-AF and the EP matrix, and the calculation results are shown in Table 5. Among them, the surface energy $\gamma_E$ of EP was 41 mJ m$^{-2}$.[39]

**Table 5. Interfacial Energy and Adhesion Work of AF and EP**

| | R-AF | PDA-AF | PEI-PDA-AF | $NH_2$-CNTs-PEI-PDA-AF |
|---|---|---|---|---|
| contact angle (degree) | 75.4 | 69.0 | 63.6 | 58.9 |
| interfacial energy (mJ m$^{-2}$) | 23.6 | 39.2 | 47.2 | 50.8 |
| adhesion work (mJ m$^{-2}$) | 51.3 | 55.8 | 59.5 | 62.3 |

As can be seen from Table 5, after gradual modification, the interfacial energy and adhesion work between the AF and EP matrix are gradually improved. Among them, $NH_2$-CNTs-PEI-PDA-AF has the maximum interfacial energy and adhesion work of 50.8 and 62.3 mJ m$^{-2}$, which are 115 and 21.4% higher than those of R-AF, respectively. It is beneficial to improve the interfacial bond strength and mechanical properties of the aramid fiber/epoxy resin composites.

**3.4. Monofilament Tensile Properties of the Aramid Fiber.** As the reinforcing phase of composites, the aramid fiber is the main carrier of external load, and its strength directly determines the mechanical properties of composites. Therefore, in this paper, the effect of modification treatment on fiber body strength was studied by testing the monofilament tensile strength of AF in different modification stages. The internal defects such as impurities and directional microcrystals produced during aramid fiber processing weaken the monofilament tensile strength of the fibers.[40] At the same time, some modification processes will produce etching on the aramid fiber because of chemical reaction, destroy the surface structure of the aramid fiber, and form defects such as holes and cracks. When an external load is applied on the fiber surface, stress concentration is easily formed at the defect, which might fracture the fiber under a small load. Therefore, the monofilaments' tensile strength of the aramid fiber shows great dispersion. The Weibull distribution function[41−43] can be used for statistical analysis of test data.

The experimental data of 12 samples of four kinds of fibers (R-AF, PDA-AF, PEI-PDA-AF, $NH_2$-CNTs-PEI-PDA-AF) were measured, and the tensile distance was all 20 mm. The least-square method was used to estimate the parameters of these data, and Weibull shape parameters and scale parameters were obtained by linear fitting calculation. The expression of the one-dimensional two-parameter Weibull distribution function[44] is shown in formula 10.

$$F(\sigma_f) = 1 - \exp\left[-L\left(\frac{\sigma_f}{\sigma_0}\right)^m\right] \quad (10)$$

In formula (10), $\sigma_f$ is the tensile strength of a single aramid fiber; $L$ is the tensile distance; $F(\sigma_f)$ is when the tensile



https://doi.org/10.1021/acsomega.2c03390
ACS Omega 2022, 7, 35610−35625

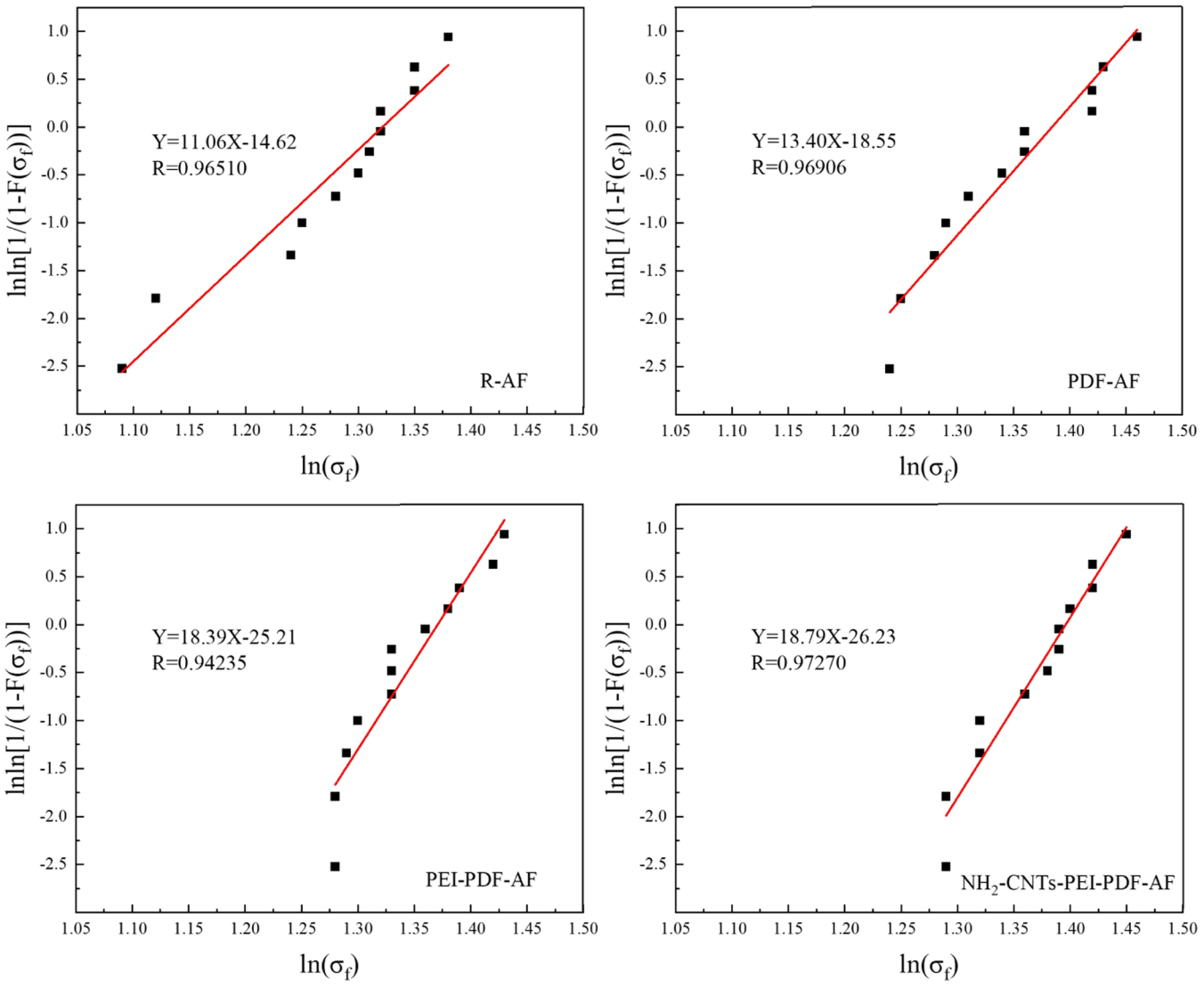


**Figure 10.** Weibull distribution curve of AF monofilament tensile strength.

distance is $L$, the cumulative distribution function of the fracture probability of the aramid fiber when the fracture stress is not higher than $\sigma_f$, that is, the failure probability; $\sigma_0$ is the scale parameter of the Weibull distribution at tensile distance; and $m$ is the shape parameter of the Weibull distribution, also known as the Weibull modulus, which is the internal characterization parameter of the fiber. $m$ and $\sigma_0$ are collectively called Weibull parameters.

$$P = 1 - F(\sigma_f) = \exp\left[-L\left(\frac{\sigma_f}{\sigma_0}\right)^m\right] \tag{11}$$

In formula 11, $P$ is the probability of survival. Taking the natural logarithm of both sides of eqs 11, eq 12 can be obtained.

$$\ln\ln[1/(1 - F(\sigma_f))] = m \ln \sigma_f + \ln L - \ln \sigma_0^m \tag{12}$$

It can be seen from formula 12 that $\ln\ln[1/(1 - F(\sigma_f))]$ is linear to $\ln \sigma_f$, and the least-square method[45] can be used to estimate the Weibull parameters $m$ and $\sigma_0$.

The specific steps of the least-square method are as follows. First, the monofilament tensile strength of a batch of $N$ single aramid fiber samples was determined by conventional testing techniques. The test monofilament tensile strength data were arranged in an increasing sequence from small to large: $\sigma_1 < \sigma_2 < \cdots \le \sigma_i \le \cdots \le \sigma_N$, where $\sigma_i$ represents the test strength of any sample.

The material failure probability $F(\sigma_f)$ can be calculated by formula 13 as follows

$$F(\sigma_f) = i/(N + 1) \tag{13}$$

In formula 13, $N$ is the total number of aramid fiber samples tested and $i$ is the serial number of the tested monofilament tensile strength data in an ascending order. Then, $N$ pairs of $(F(\sigma_f), \sigma_f)$ were obtained.

The linear distribution of formula 12 can be obtained as follows

$$Y = \ln\ln[1/(1 - F(\sigma_f))] \tag{14}$$

$$A = m \tag{15}$$

$$X = \ln \sigma_f \tag{16}$$

$$B = \ln L - \ln \sigma_0^m \tag{17}$$

In this way, linear regression analysis of $N$ pairs of dates $(F(\sigma_f), \sigma_f)$ was performed using the least-squares method. The



https://doi.org/10.1021/acsomega.2c03390
ACS Omega 2022, 7, 35610−35625

relationship between $\ln \ln[1/(1 - F(\sigma_f))]$ and $\ln \sigma_f$ is fitted to a straight line $Y = AX + B$; the Weibull parameters $\sigma_0$ and $m$ of the material can be obtained by solving formulas 15, 17, and 18.

$$\sigma_0 = \exp((\ln L - B)/m) \tag{18}$$

The average tensile strength of the aramid fiber monofilament can be calculated by formula 19 as follows

$$\bar{\sigma} = \sigma_0 L^{-1/m} \Gamma(1 + 1/m) \tag{19}$$

In formula 19, $\Gamma$ means the gamma function.

Figure 10 shows the Weibull distribution curve of the monofilament tensile strength of AF in different modification stages. It can be seen that the linear fitting of test data is good, which indicates that the monofilaments' stretching data of AF samples follow the Weibull distribution theory. Weibull distribution parameters of AF in different modification stages are shown in Table 6. $m$ and $\sigma_0$ are the inherent constants of the tested AF. The scale parameter $\sigma_0$ is used to characterize the tensile strength of the monofilament in Weibull analysis. The larger the scale parameter is, the larger the monofilament tensile strength is; otherwise, the smaller the monofilament tensile strength is.

**Table 6. Weibull Distribution Parameters of AF Monofilament Tensile Strength**

| Weibull distribution parameters | R-AF | PDA-AF | PEI-PDA-AF | $NH_2$-CNTs-PEI-PDA-AF |
|---|---|---|---|---|
| $B$ | −14.62 | −18.55 | −25.21 | −26.23 |
| $A = m$ | 11.06 | 13.40 | 18.39 | 18.79 |
| $R$ | 0.97 | 0.97 | 0.94 | 0.97 |
| $\sigma_0$ (GPa) | 2.64 | 2.97 | 3.19 | 3.29 |

The average monofilament tensile strength of AF in different modification stages can be further calculated by formula 19, as shown in Figure 11. It can be seen that the monofilament tensile strength of R-AF is 3.60 GPa. The monofilament tensile strengths of PDA-AF and PEI-PDA-AF were 3.76 and 3.78 GPa, respectively, slightly higher than that of R-AF. These results indicated that the dopamine autopolymerization reaction and PEI addition reaction were mild and did not damage the microstructure of the AF surface. At the same time, the coating effect of PDA and PEI on the AF surface fills the defect of the fiber surface, alleviates the stress concentration effect caused by the fiber under longitudinal tensile load, and thus improves the AF monofilament tensile strength. After further deposition of $NH_2$-CNTs, the monofilament tensile strength of $NH_2$-CNTs-PEI-PDA-AF was 3.89 GPa, 8.1% higher than that of R-AF. This is due to the excellent mechanical properties of carbon nanotubes themselves, and the average tensile strength of different types of carbon nanotubes is above 60 GPa. Therefore, the introduction of $NH_2$-CNTs improves the monofilament tensile strength of aramid fibers.

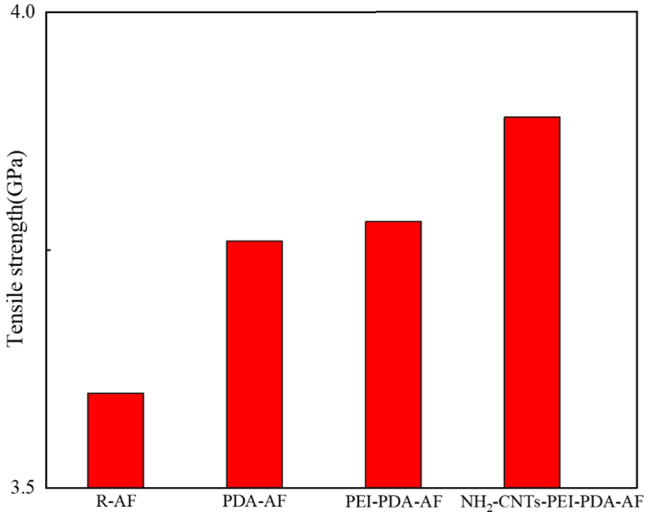


**Figure 11.** Average monofilament tensile strength of AF.

**3.5. Interlaminar Shear Strength (ILSS) and Bending Strength ($\sigma_B$) of Aramid Fiber-Reinforced Epoxy Resin Matrix Composites.** To analyze and evaluate the interface properties and mechanical properties of aramid fiber-reinforced epoxy resin composites, in this paper, ILSS and $\sigma_B$ of the composites at different modification stages were tested by the three-point bending method according to ASTM D2344 and ASTM D7264 standards, respectively. The test results are shown in Figures 12 and 13, respectively.

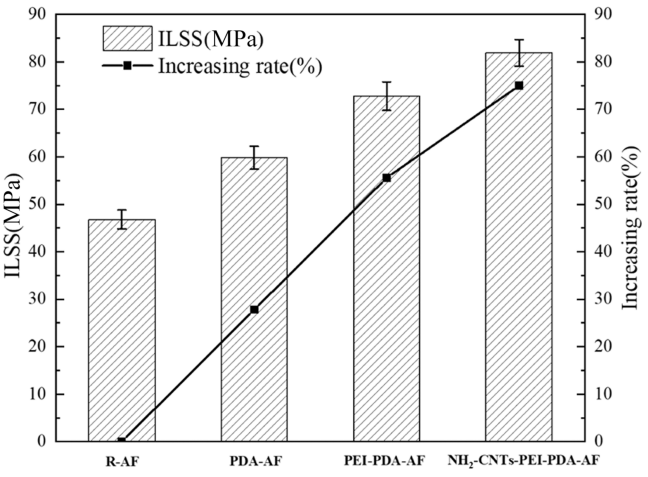


**Figure 12.** ILSS between AF and EP.

As can be seen from Figure 12, the ILSS between R-AF and EP is 46.8 MPa. After deposition of PDA, the ILSS between PDA-AF and EP is 59.8 MPa, which is 27.8% higher than that

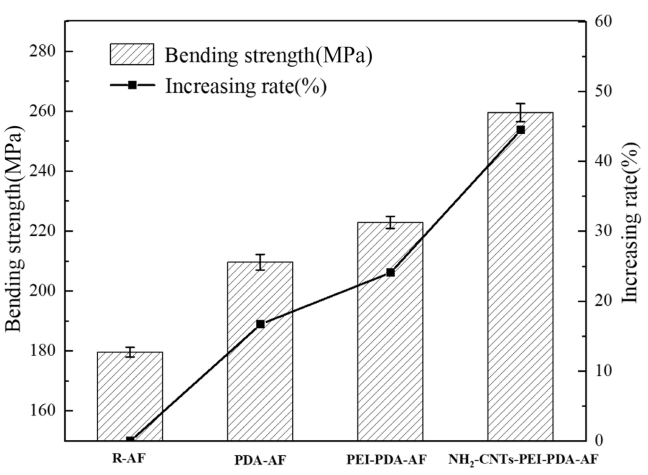


**Figure 13.** Bending strength of AF/EP composites.



https://doi.org/10.1021/acsomega.2c03390
ACS Omega 2022, 7, 35610−35625

of R-AF. After further deposition of PEI, the ILSS between PEI-PDA-AF and EP reaches 72.8 MPa, which is 55.6% higher than that of R-AF. In particular, the ILSS between $NH_2$-CNTs-PEI-PDA-AF and EP was a maximum of 81.9 MPa, which was significantly increased by 75% compared with R-AF. This is because the wettability between $NH_2$-CNTs-PEI-PDA-AF and the EP matrix is significantly improved (the contact angle is the minimum, which is 21.9% lower than that of R-AF) and the interface properties are greatly improved (the interface energy and adhesion energy reach the maximum, which are 115 and 21.4% higher those of R-AF, respectively). Therefore, the ILSS between $NH_2$-CNTs-PEI-PDA-AF and the EP matrix was significantly increased.

In the same way, Figure 13 shows that the bending strength $\sigma_B$ of R-AF/EP is 179.6 MPa. After deposition of PDA, the $\sigma_B$ of PDA-AF/EP is 209.6 MPa, which is 16.7% higher than that of R-AF/EP. After further deposition of PEI, the $\sigma_B$ of PEI-PDA-AF/EP reaches 222.9 MPa, which is 24.1% higher than that of R-AF/EP. In particular, the $\sigma_B$ of $NH_2$-CNTs-PEI-PDA-AF/EP is the maximum (259.5 MPa), which is 44.5% higher than that of R-AF/EP. The reason is that the surface chemical composition of AF changes significantly due to the layer-by-layer modification treatment, and the active groups increase. The gradually abundant active functional groups on the surface of AF can be used to form chemical bonds with the epoxy resin, so as to bond with the resin more firmly. At the same time, the surface roughness of AF increases obviously, which is conducive to the infiltration of the resin and the formation of mechanical locking. Therefore, the improvement in interface properties between the fiber and the matrix is conducive to the improvement of mechanical properties, thus significantly improving the bending strength of composites.

**3.6. Tensile Strength ($\sigma_t$) and Analysis of the Tensile Section of Aramid Fiber-Reinforced Epoxy Resin Matrix Composites.** The tensile strength $\sigma_t$ of AF/EP composite was tested according to ASTM D3039. The results are shown in Figure 14. It can be seen that the tensile strength of AF (PDA-AF, PEI-PDA-AF, and NH2-CNT-PEI-PDA-AF)-enhanced epoxy composites gradually increased after layer-by-layer modification. For example, R-AF/EP without surface treatment has a $\sigma_t$ of 415 MPa. After deposition of PDA, the $\sigma_t$ of PDA-AF/EP is 442 MPa, which is 6.5% higher than that of R-AF/EP. After further deposition of PEI, the $\sigma_t$ of PEI-PDA-AF/EP reaches 460 MPa, which is 10.8% higher than that of R-AF/EP. In particular, when $NH_2$-CNTs were successfully grafted onto the fiber surface, the enhancement effect of $NH_2$-CNTs-PEI-PDA-AF/EP was the best, and the $\sigma_t$ of $NH_2$-CNTs-PEI-PDA-AF/EP was the highest (477 MPa), which was 14.9% higher than that of R-AF/EP, significantly improving the strength of the epoxy composite.

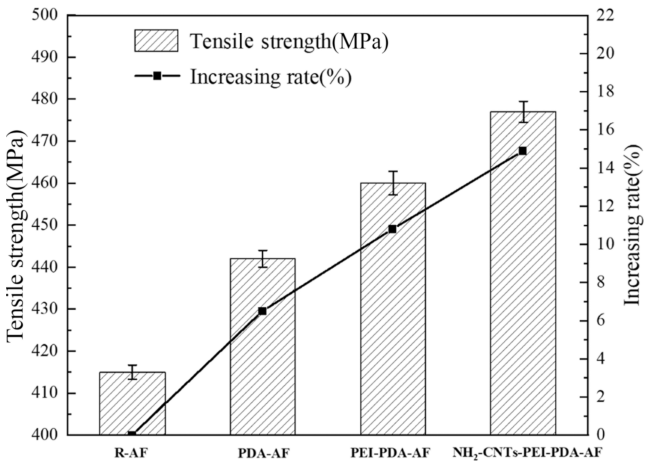


**Figure 14.** Tensile strength of the AF/EP composite.

By observing the microstructure of the tensile section of AF/EP composites at different modification stages by SEM, the strengthening mechanism and failure mechanism of fiber composites can be further analyzed. The microscopic morphology of the tensile section of AF/EP composites at different modification stages is shown in Figure 15. It can be seen that R-AF and the EP matrix are almost completely debonded, the fiber surface is relatively smooth with almost no resin bonded on it (Figure 15a), and a very smooth channel is formed (as indicated by the green arrow in Figure 15a), which is the trace left after the fiber is completely pulled out. At the same time, some large EP fragments are produced on the fiber surface, which is a typical characteristic of brittle fracture (as indicated by the blue dotted arrow in Figure 15a). This is because the wettable property between R-AF and EP without surface treatment is poor (contact angle 75.4°), and the interface energy and adhesion work between R-AF and EP are relatively low (23.6 and 51.3 mJ $m^{-2}$, respectively), resulting in poor interface adhesion property between R-AF and EP; moreover, the load cannot be effectively transferred to the aramid fiber through the resin matrix. The carrying capacity of the aramid fiber is not fully developed. Therefore, the tensile strength of the R-AF/EP composite is relatively low (415 MPa), and its failure mode is mainly interface debonding failure.

Figure 15b is the SEM photo of the tensile section of PDA-AF/EP. It can be seen that the section morphology has changed significantly, and a large number of fine fragmented epoxy resin matrixes are adhered to the fiber surface (the area marked by blue circles in Figure 15b). Moreover, many viscous epoxy resin attachments (indicated by the red arrow in Figure 15b) are embedded between the fiber surfaces, which produce certain plastic deformation. This is because PDA has good adhesion characteristics, and the wettability between AF and EP is improved (contact angle 69.0°, surface energy 39.2 mJ $m^{-2}$, adhesion power 55.8 mJ $m^{-2}$) after the deposition of PDA on the AF surface by the dopamine polymerization reaction; moreover, the interface bonding strength is improved. More fibers were used to carry the load under the load; therefore, the tensile strength of the composite increased (442 MPa).

Figure 15c shows the morphology of the tensile section of PEI-PDA-AF/EP. It can be seen that all of the fiber surfaces are coated with resin, and a large amount of resin is filled between the fibers. The resin distribution is relatively uniform, and the fiber is closely combined with the resin matrix. The surface of PEI-PDA-AF/EP showed some large debris, which produced certain plastic deformation (indicated by the red dotted arrow in Figure 15c). At the same time, a large number of stretched broken fiber filaments in the AF fiber bundle (shown by the blue arrow in Figure 15c) also appeared on the surface, indicating that the fiber is damaged under load. This is because after surface deposition of PEI-PDA, on the one hand, the wettability between AF and EP was effectively improved; on the other hand, due to the introduction of a large number of active groups such as amino groups, the interface bonding


https://doi.org/10.1021/acsomega.2c03390
ACS Omega 2022, 7, 35610−35625

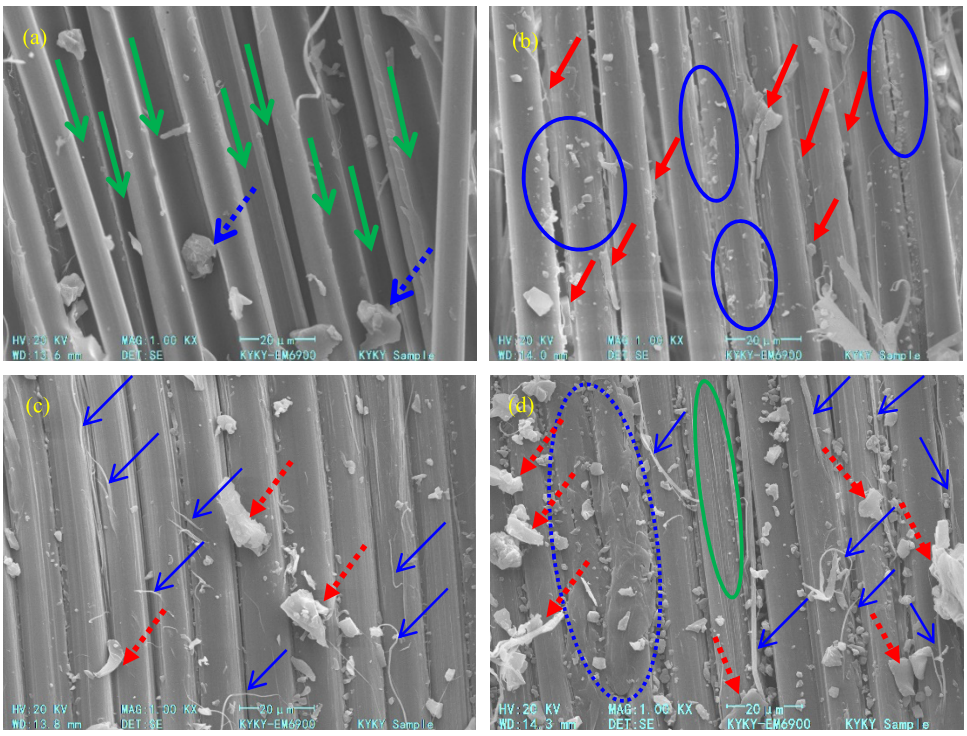


**Figure 15.** Tensile section morphology of AF/EP composites: (a) R-AF/EP, (b) PDA-AF/EP, (c) PEI-PDA-AF/EP, and (d) $NH_2$-CNTs-PEI-PDA-AF/EP.

strength between the fiber and the matrix is improved. When the composite is subjected to an external load, the resin matrix can transfer the load to the aramid fiber more effectively, and the fiber has a stronger carrying capacity, which gives full play to the strengthening effect of the fiber. Therefore, the PEI-PDA-AF/EP composite exhibits high tensile strength (460 MPa) under a load.

In particular, compared with the surface of PEI-PDA-AF/EP, $NH_2$-CNTs-PEI-PDA-AF was closely bound to the EP matrix, and more massive detrital particles were generated on the surface. The number of large and small detrital particles increased significantly, and the degree of plastic deformation caused by large detrital particles was more obvious (as shown by the red dotted arrow in Figure 15d). At the same time, an obvious sticky and dense covering layer was observed on the fiber surface (marked by blue dotted circles in Figure 15d), and shear plasticization marks of the EP matrix were also produced on the fiber bundle surface (marked by green circles in Figure 15d). In addition, relatively thick strips were formed on the surface of $NH_2$-CNTs-PEI-PDA-AF/EP (indicated by the blue arrow in Figure 15d), which may be the combination of some fiber silk in the AF fiber bundle as well as $NH_2$-CNTs-PEI-PDA deposited on the surface and the EP matrix. This is because of the following reasons. (1) The surface modification layer of $NH_2$-CNTs-PEI-PDA-AF introduces a large number of active groups such as $-NH_2$ and $-OH$, which can form stable covalent bonds with the EP matrix through ring-opening polymerization (as shown in Figure 16), thereby improving the chemical bonding between the fibers and the epoxy resin matrix. At the same time, the large amount of $NH_2$-CNTs deposited on the fiber surface effectively increased the surface roughness of the fibers and improved the mechanical meshing between the fibers and the epoxy resin matrix. The enhancement of the above two aspects made the $NH_2$-

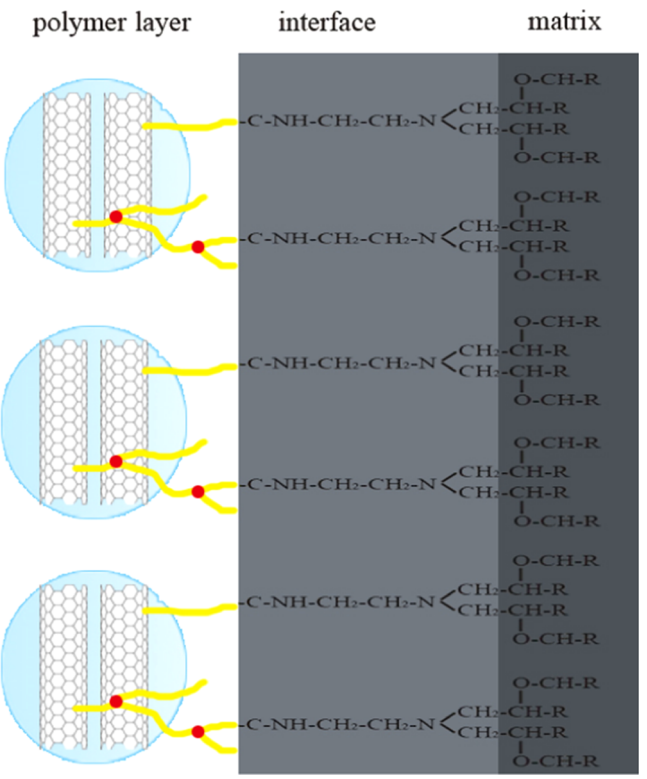


**Figure 16.** Interfacial molecular structure of the $NH_2$-CNTs-PEI-PDA layer and the EP matrix.

CNTs-PEI-PDA-AF surface-modified layer significantly improve the contact angle between AF and the EP matrix (58.9°); increased the AF surface energy (50.8 mJ $m^{-2}$) and adhesion energy (62.3 mJ $m^{-2}$); and improved the interfacial bonding strength between the fiber and the matrix (ILSS was



https://doi.org/10.1021/acsomega.2c03390
ACS Omega 2022, 7, 35610−35625

81.9 MPa). (2) A large number of PDA/PEI/$NH_2$-CNTs multilayer films deposited on the fiber surface are similar to the flexible layers (Figure 16), which play a role in strengthening and toughing the EP matrix in the interface area. In the loading process, the matrix produced certain plastic deformation and effectively absorbed the energy, so that the load could be more effectively transferred from the resin matrix to the fiber, and AF was more evenly loaded. The mechanical properties of $NH_2$-CNTs-PEI-PDA-AF/EP were significantly improved (tensile strength 477 MPa).

## 4. CONCLUSIONS

To improve the mechanical properties of AF/EP composites, a green and efficient surface modification method was proposed, and PDA/PEI/$NH_2$-CNT multilayer films were successfully deposited on the AF surface. The modified PDA-AF, PEI-PDA-AF, and $NH_2$-CNTs-PEI-PDA-AF were prepared separately. The deposition process of the multilayer film was verified, and the effect of modification on the structure and performance of AF was studied. The results show that the interfacial properties and mechanical properties of the composites are gradually improved with the successful deposition of PDA, PEI, and $NH_2$-CNTs layer by layer. $NH_2$-CNTs-PEI-PDA-AF showed the best modification enhancement effect. Compared with R-AF, the monofilament tensile strength of $NH_2$-CNTs-PEI-PDA-AF increased by 8.1%, the contact angle with EP decreased by 21.9%, the interface energy and adhesion energy increased by 115 and 21.4%, respectively, and the ILSS, bending strength, and tensile strength of $NH_2$-CNTs-PEI-PDA-AF/EP increased by 75, 44.5, and 14.9%, respectively. The enhancement of the mechanical properties of $NH_2$-CNTs-PEI-PDA-AF/EP was due to the significant improvement of the interface bonding strength between the AF and EP. On the one hand, the introduction of a large number of active groups such as amino groups on the AF surface formed stable covalent bonds with the epoxy matrix. On the other hand, the large number of $NH_2$-CNTs deposited on the AF surface effectively increased the surface roughness of AF, thereby strengthening the mechanical meshing between the fibers and the EP matrix. Moreover, the surface-modified layer can strengthen and toughen the EP matrix in the interface region, which can make the EP matrix produce certain plastic deformation and absorb energy in the process of loading. Therefore, the multilayer structure of $NH_2$-CNTs-PEI-PDA-AF prepared can effectively enhance the mechanical properties of epoxy composites and will have great application potential in the preparation of high-performance fiber-reinforced composites.

## AUTHOR INFORMATION


### Corresponding Author

**Lizhou An** − *College of Field Engineering, Army Engineering University of PLA, Nanjing 210007 Jiangsu, China*; Email: 44474922@qq.com

### Authors

**Ting Xu** − *College of Field Engineering, Army Engineering University of PLA, Nanjing 210007 Jiangsu, China*; orcid.org/0000-0002-0369-0030

**Jin Tian** − *College of Field Engineering, Army Engineering University of PLA, Nanjing 210007 Jiangsu, China*

**Yumin Jiao** − *Unit 94789 of PLA, Nanjing 210018 Jiangsu, China*

**Qin Yin** − *College of Field Engineering, Army Engineering University of PLA, Nanjing 210007 Jiangsu, China*

**Yefa Tan** − *College of Field Engineering, Army Engineering University of PLA, Nanjing 210007 Jiangsu, China*; orcid.org/0000-0003-1996-6190

Complete contact information is available at: https://pubs.acs.org/10.1021/acsomega.2c03390



### Funding

The funding source for this work is the Natural Science Foundation of China, project number: 51708553.


### Notes

The authors declare no competing financial interest.

## ACKNOWLEDGMENTS

The authors thank Dr. Tian Jin and Dr. Anli Zhou for their guidance and help in the experimental operation and writing of the paper. They also thank Professor Tan Yefa for his guidance in the revision of the paper. The authors thank the other authors for all kinds of help in work and life.

## REFERENCES


(1) Gao, J.; Yang, X.; Huang, L. H. Numerical prediction of mechanical properties of rubber composites reinforced by aramid fiber under large deformation. *Compos. Struct.* **2018**, *201*, 29−37.

(2) Ramasamy, N.; Arumugam, V.; Suresh Kumar, C. Characterization of fiber/matrix interfacial bonding strength of chemically grafted aramid fiber surface with epoxy resin composites. *Polym. Compos.* **2021**, *1*, 399−410.

(3) Cheng, Z.; Li, X.; Lv, J.; Liu, Y.; Liu, X. Constructing a new tear-resistant skin for aramid fiber to enhance composites interfacial performance based on the interfacial shear stability. *Appl. Surf. Sci.* **2021**, *544*, No. 148953.

(4) Pratibha, D.; Sreekara Reddy, M. B. S.Aramid fiber as potential reinforcement for polymer matrix composites: a review*Emergent Mater.***2021**, *441*, DOI: 10.1007/s42247-021-00246-x.

(5) Wang, Y.; Qu, R.; Pan, F.; Jia, X.; Sun, C.; Ji, C.; et al. Preparation and characterization of thiol- and amino-functionalized polysilsesquioxane coated poly(p-phenylenetherephthal amide) fibers and their adsorption properties towards Hg(II). *Chem. Eng. J.* **2017**, *317*, 187−203.

(6) Wang, W.; Li, R.; Tian, M.; Liu, L.; Zou, H.; Zhao, X.; Zhang, L. Surface silverized meta-aramid fibers prepared by bio-inspired polydopamine functionalization. *ACS Appl. Mater. Interfaces* **2013**, *5*, 2062−2069.

(7) Gómez-del Río, T.; Salazar, A.; Pearson, R. A.; Rodriguez, J. Fracture behaviour of epoxy nanocomposites modified with triblock copolymers and carbon nanotubes. *Composites, Part B* **2016**, *87*, 343−349.

(8) Liu, T.-M.; Zheng, Y.; Hu, J. Surface Modification of Aramid Fibers with New Chemical Method for Improving Interfacial Bonding Strength with Epoxy Resin. *J. Appl. Polym. Sci.* **2010**, *118*, 2541−2552.

(9) Ehlert, G. J.; Lin, Y.; Sodano, H. A. Carboxyl Functionalization of Carbon Fibers Through a Grafting Reaction that Preserves Fiber Tensile Strength. *Carbon* **2011**, *49*, 4246−4255.

(10) Yang, X.; Tu, Q.; Shen, X.; Pan, M.; Jiang, C.; Zhu, P.; Hu, C.; et al. Surface modification of Poly(p-phenylene terephthalamide) fibers by polydopamine-polyethyleneimine/graphene oxide multilayer films to enhance interfacial adhesion with rubber matrix. *Polym. Test.* **2019**, *78*, No. 105985.

(11) Zeng, L.; Liu, X.; Chen, X.; Soutis, C. Surface Modification of Aramid Fibres with Graphene Oxide for Interface Improvement in Composites. *Appl. Compos. Mater.* **2018**, *25*, 843−852.

(12) Sun, Z.; Shi, S.; Hu, X.; Chen, H.; Wong, Z. Adhesive Joints Between Carbon Fiber and Aluminum Foam Reinforced by Surface-Treated Aramid Fibers. *Polym. Compos.* **2015**, *36*, 192−197.

(13) Li, S.; Han, K.; Rong, H.; Li, X.; Yu, M. Surface modification of aramid fibers via ammonia-plasma treatment. *J. Appl. Polym. Sci.* **2013**, *131*, No. 40250.
(14) Zhao, F.; Huang, Y.; Liu, L.; Bai, Y.; Xu, L. Formation of a carbon fiber/polyhedral oligomeric silsesquioxane/carbon nanotube hybrid reinforcement and its effect on the interfacial properties of carbon fiber/epoxy composites. *Carbon* **2011**, *49*, 2624−2632.
(15) Mei, L.; He, X.; Li, Y.; Wang, R.; Wang, C.; Peng, Q. Grafting carbon nanotubes onto carbon fiber by use of dendrimer. *Mater. Lett.* **2010**, *64*, 2505−2508.
(16) Yang, X.; Tu, Q.; Shen, X.; Zhu, P.; Li, Y.; Zhang, S. A novel method for deposition of multi-walled carbon nanotubes onto poly (p-phenylene terephthalamide) fibers to enhance interfacial adhesion with rubber matrix. *Polymers* **2019**, *11*, No. 374.
(17) Lee, H.; Dellatore, S. M.; Miller, W. M.; Messersmith, P. B. Mussel-Inspired Surface Chemistry for Multifunctional Coatings. *Science* **2007**, *318*, 426−430.
(18) Jiang, J.; Zhu, L.; Zhu, L.; Zhu, B.; Xu, Y. Surface characteristics of a self-polymerized dopamine coating deposited on hydrophobic polymer films. *Langmuir* **2011**, *27*, 14180−14187.
(19) Chen, S.; Cao, Y.; Feng, J. Polydopamine As an Efficient and Robust Platform to Functionalize Carbon Fiber for High-Performance Polymer Composites. *ACS Appl. Mater. Interfaces* **2014**, *6*, 349−356.
(20) Xu, C.; Tian, M.; Liu, L.; Zou, H.; Zhang, L.; Wang, W. Fabrication and Properties of Silverized Glass Fiber by Dopamine Functionalization and Electroless Plating. *J. Electrochem. Soc.* **2012**, *159*, D217−D224.
(21) Tian, J.; Zhang, H.; Liu, M.; Deng, F.; Huang, H.; Wan, Q.; Li, Z.; Wang, K.; He, X.; Zhang, X.; Wei, Y. A bioinspired strategy for surface modification of silica nanoparticles. *Appl. Surf. Sci.* **2015**, *357*, 1996−2003.
(22) Zhang, X.; Zeng, G.; Tian, J.; Wan, Q.; Huang, Q.; Wang, K.; et al. PEGylation of carbon nanotubes via mussel inspired chemistry: Preparation, characterization and biocompatibility evaluation. *Appl. Surf. Sci.* **2015**, *351*, 425−432.
(23) Qi, Z.; Tan, Y.; Wang, H.; Xu, T.; Wang, L.; Xiao, C. Effects of noncovalently functionalized multiwalled carbon nanotube with hyperbranched polyesters on mechanical properties of epoxy composites. *Polym. Test.* **2017**, *64*, 38−47.
(24) Wang, L.; Tan, Y.; Wang, X.; Xu, T.; Xiao, C.; Qi, Z. Mechanical and fracture properties of hyperbranched polymer covalent functionalized multiwalled carbon nanotube-reinforced epoxy composites. *Chem. Phys. Lett.* **2018**, *706*, 31−39.
(25) Tian, J.; Tan, Y.; Zhang, Z.; Wang, X.; Xu, T.; Tang, B. Effects of hyperbranched polyesters covalent functionalized multiwalled carbon nanotubes on the mechanical and tribological properties of epoxy composites. *Mater. Res. Express* **2020**, *7*, No. 015302.
(26) Feng, X.; Qiao, J.; et al. Surface modification of UHMWPE fiber by bionic modification of dopamine and secondary functionalization of polyethylene imine. *J. TJPU* **2016**, *35*, 14−19.
(27) Liebscher, J.; Mrówczyński, R.; Scheidt, H. A.; Filip, C.; Hădade, N. D.; Turcu, R.; Bende, A.; Beck, S. Structure of polydopamine: a never-ending story. *Langmuir* **2013**, *29*, 10539−10548.
(28) Liu, Y.; Ai, K.; Lu, L. Polydopamine and Its Derivative Materials: Synthesis and Promising Applications in Energy, Environmental, and Biomedical Fields. *Chem. Rev.* **2014**, *114*, 5057−5115.
(29) Sharma, S.; Pathak, A. K.; Singh, V. N.; Teotia, S.; Dhakate, S. R.; Singh, B. P. Excellent mechanical properties of long multiwalled carbon nanotube bridged Kevlar fabric. *Carbon* **2018**, *137*, 104−117.
(30) Chen, Y.; Yin, Q.; Zhang, X.; Zhang, W.; Jia, H.; Ji, Q.; Yang, F.; Rui, X. Rational design of multifunctional properties for styrene-butadiene rubber reinforced by modified Kevlar nanofibers. *Composites, Part B* **2019**, *166*, 196−203.
(31) Yang, X.; Tu, Q.; Shen, X.; Yin, Q.; Pan, M.; Jiang, C.; Hu, C. Enhancing the interfacial adhesion with rubber matrix by grafting polydopamine-carbon nanotubes onto poly(p-phenylene terephthalamide) fibers. *Polymers* **2019**, *11*, No. 1231.
(32) Wang, L.; Shi, Y.; Chen, S.; Wang, W.; Tian, M.; Ning, N.; Zhang, L. Highly efficient mussel-like inspired modification of aramid fibers by UV-accelerated catechol/polyamine deposition followed chemical grafting for high-performance polymer composites. *Chem. Eng. J.* **2017**, *314*, 583−593.
(33) Liu, Y.; Fang, Y.; Liu, X.; Wang, X.; Yang, B. Mussel-inspired modification of carbon fiber via polyethyleneimine/polydopamine co-deposition for the improved interfacial adhesion. *Compos. Sci. Technol.* **2017**, *151*, 164−173.
(34) Tian, J.; Xu, T.; Zhang, Z.; An, L.; Li, X.; Tan, Y. Study on the construction of polyethyleneimine/nano-silica multilayer film on the carbon fiber surfaces to improve the interfacial properties of carbon fiber/epoxy composites. *Compos. Interfaces* **2021**, *29*, 361−381.
(35) Sa, R.; Yan, Y.; Wei, Z.; Zhang, L.; Wang, W.; Tian, M. Surface Modification of Aramid Fibers by Bio-Inspired Poly(dopamine) and Epoxy Functionalized Silane Grafting. *ACS Appl. Mater. Interfaces* **2014**, *6*, 21730−21738.
(36) Tran, M. Q.; Ho, K. K. C.; Kalinka, G.; Shaffer, M. S. P.; Bismarck, A. Carbon Fiber Reinforced Poly(vinylidene fluoride): Impact of Matrix Modification on Fiber/Polymer Adhesion. *Compos. Sci. Technol.* **2008**, *68*, 1766−1776.
(37) Schrader, M. E. Young-Dupre Revisited. *Langmuir* **1995**, *11*, 3585−3589.
(38) Owens, D. K.; Wendt, R. C. Estimation of the surface free energy of polymers. *J. Appl. Polym. Sci.* **1969**, *13*, 1741−1747.
(39) Weldon, D. G. Failure Analysis of Paints and Coatings. *Pigm. Resin Technol.* **2007**, *36*, No. 2.
(40) Zhang, R. L.; Gao, B.; Ma, Q. H.; Zhang, J.; Cui, H. Z.; Liu, L. Directly grafting graphene oxide onto carbon fiber and the effect on the mechanical properties of carbon fiber composites. *Mater. Des.* **2016**, *93*, 364−369.
(41) Zhou, Y.; Li, W.WEIBULL analysis and Study on monofilament strength of carbon fiber*High-Tech Fibers and Applications*2015, *6*, 3540.
(42) Wang, C.; Xie, J.; Qiu, Y. WEIBULL theory was used to evaluate the effect of surface treatment on tensile strength of carbon fibers. *Ind. Text.* **2011**, *2*, 19−22.
(43) Wang, H.; Wang, J.; Huang, Z.; Zhu, J. WEIBULL was used to evaluate the effect of surface treatment on glass fiber strength. *J. WUT* **2003**, *6*, 13−15.
(44) Sakin, R.; Ay, I. Statistical analysis of bending fatigue life data using Weibull distribution in glass-fiber reinforced polyester composites. *Mater. Des.* **2008**, *29*, 1170−1181.
(45) Gong, J.; Li, Y. Statistical properties of least squares estimator of WEIBULL modulus for ceramic materials. *J. Ceram.* **1997**, *18*, 145−150.


https://doi.org/10.1021/acsomega.2c03390
*ACS Omega* 2022, 7, 35610−35625